Atomic Layer Deposition of Yttria-Stabilized Zirconia for Solid Oxide Fuel Cells

4 AUTHORS, INCLUDING:

Cheng-Chieh Chao
Stanford University

19 PUBLICATIONS **541** CITATIONS

SEE PROFILE

Hong Huang
Wright State University

48 PUBLICATIONS **1,133** CITATIONS

SEE PROFILE

Atomic Layer Deposition of Yttria-Stabilized Zirconia for Solid Oxide Fuel Cells

Joon Hyung Shim,*,† Cheng-Chieh Chao,† Hong Huang,† and Fritz B. Prinz†,‡

Department of Mechanical Engineering and Department of Material Science and Engineering,
Stanford University, Stanford, California 94305

Yttria-stabilized zirconia (YSZ) films were synthesized by atomic layer deposition (ALD). Tetrakis-(dimethylamido)zirconium and tris(methylcyclopentadienyl)yttrium were used as ALD precursors with distilled water as oxidant. From X-ray photoelectron spectroscopy (XPS) compositional analysis, the yttria content was identified to increase proportionally to the pulse ratio of Y/Zr. Accordingly, the target stoichiometry $ZrO_2/Y_2O_3 = 0.92:0.08$ was achieved. Crystal and grain structures of ALD YSZ films grown on amorphous Si_3N_4 were analyzed by X-ray diffraction (XRD) and atomic force microscopy (AFM). The microstructure of the polycrystalline films consisted of grains of tens of nanometers in diameter. To evaluate ALD YSZ films as oxide ion conductor, freestanding 60 nm films were prepared with porous platinum electrodes on both sides of the electrolyte. This structure served as a solid oxide fuel cell designed to operate at low temperatures. Maximum power densities of 28 mW/cm^2, 66 mW/cm^2, and 270 mW/cm^2 were observed at 265 °C, 300 °C, and 350 °C, respectively. The high performance of thin film ALD electrolyte fuel cells is related to low electrolyte resistance and fast electrode kinetics. The exchange current density at the electrode−electrolyte interface was approximately 4 orders of magnitude higher compared to reference Pt-YSZ values.

Introduction

Yttria-stabilized zirconia (YSZ) membranes have been widely used as solid-state electrolytes for a range of applications because of their high oxide ion conductivity and good stability. However, high operating temperatures of about 1000 °C limit further expansion of applications due to thermal stresses and rapid degradation. For this reason, extensive research has been conducted to reduce electrolyte resistance at reduced temperatures, for example, by replacing YSZ with other materials such as samaria or gadolinia-doped ceria that show higher oxide ion conductivity[1−3] or by reducing the thickness of the electrolyte to lower ohmic losses.[4] Recently, enhanced ionic conductivity in nanosize electrolytes was discovered.[5,6]

Traditionally, production of nanosize YSZ films required advanced fabrication techniques such as radio frequency (RF) sputtering,[7] magnetron sputtering,[8] sol−gel spin coating,[8,10]

pulsed laser deposition (PLD)[11] and chemical vapor deposition (CVD).[12] Unlike other thin film fabrication techniques, CVD methods can achieve uniform and isotropic deposition with conformal covering over three-dimensional substrates without pinholes. Atomic layer deposition (ALD) is a modified CVD technique whereby the substrate surface is exposed alternately to different vaporized precursors. Because gaseous precursors are strictly separated from each other during deposition and the precursors have self-limiting chemistry, ideally one reaction cycle may produce one atomic layer only. For this reason, ALD can be a promising fabrication method to grow ultrathin doped oxide films because composition of ALD films can be altered at each atomic layer with desired ratios. Deposition of ternary oxides by altering different types of oxide layers using ALD has been successfully demonstrated.[13−15] Several studies have attempted fabrication of defect-containing doped oxide ion conductors.[16−18] In this paper, we present fabrication of

---
* To whom correspondence should be addressed. E-mail: shimm@stanford.edu.
† Department of Mechanical Engineering.
‡ Department of Material Science and Engineering.

(1) Doshi, R.; Richards, V. L.; Carter, J. D.; Wang, X. P.; Krumpelt, M. *J. Electrochem. Soc.* **1999**, *146*, 1273−8.
(2) Xia, C. R.; Liu, M. L. *Solid State Ionics* **2001**, *144*, 249−55.
(3) Xia, C. R.; Chen, F. L.; Liu, M. L. *Electrochem. Solid-State Lett.* **2001**, *4*, A52−4.
(4) de Souza, S.; Visco, S. J.; DeJonghe, L. C. *Solid State Ionics* **1997**, *98*, 57−61.
(5) Sata, N.; Eberman, K.; Eberl, K.; Maier, J. *Nature* **2000**, *408*, 946−9.
(6) Huang, H.; Gur, T. M.; Saito, Y.; Prinz, F. *Appl. Phys. Lett.* **2006**, *89*.
(7) Huang, H.; Nakamura, M.; Su, P.; Fasching, R.; Saito, Y.; Prinz, F. B. *J. Electrochem. Soc.* **2007**, *154*, b20−4.
(8) Wang, L. S.; Barnett, S. A. *J. Electrochem. Soc.* **1992**, *139*, 1134−40.
(9) Peshev, P.; Slavova, V. *Mater. Res. Bull.* **1992**, *27*, 1269−75.
(10) Kueper, T. W.; Visco, S. J.; De Jonghe, L. C. *Solid State Ionics* **1992**, *52*, 251−159.
(11) Kokai, F.; Amano, K.; Ota, H.; Ochiai, Y.; Umemura, F. *J. Appl. Phys.* **1992**, *72*, 699−704.
(12) Chour, K. W.; Chen, J.; Xu, R. *Thin Solid Films* **1997**, *304*, 106−12.
(13) Vehkamaki, M.; Hatanpaa, T.; Hanninen, T.; Ritala, M.; Leskela, M. *Electrochem. Solid-State Lett.* **1999**, *2*, 504−6.
(14) Nieminen, M.; Sajavaara, T.; Rauhala, E.; Putkonen, M.; Niinisto, L. *J. Mater. Chem.* **2001**, *11*, 2340−5.
(15) Hatanpaa, T.; Vehkamaki, M.; Mutikainen, I.; Kansikas, J.; Ritala, M.; Leskela, M. *Dalton Trans.* **2004**, 1181−8.
(16) Asikainen, T.; Ritala, M.; Leskela, M. *J. Electrochem. Soc.* **1995**, *142*, 3538−41.
(17) Putkonen, M.; Sajavaara, T.; Niinisto, J.; Johansson, L. S.; Niinisto, L. *J. Mater. Chem.* **2002**, *12*, 442−8.
(18) Gourba, E.; Ringuede, A.; Cassir, M.; Billard, A.; Paivasaari, J.; Niinisto, J.; Putkonen, M.; Niinisto, L. *Ionics* **2003**, *9*, 15−20.

ultrathin YSZ electrolyte films by ALD and test their quality with the help of solid oxide fuel cells for the first time. We found that low electrolyte resistance and high exchange current densities of ALD YSZ films can lead to power densities of solid oxide fuel cells in excess of 200 mW/cm^2 at temperatures well below 400 °C.

Experimental Section

For ZrO_2 and Y_2O_3 deposition, commercial tetrakis(dimethyla-mido)zirconium ($Zr(NMe_2)_4$) and tris(methylcyclopentadienyl)-yttrium ($Y(MeCp)_3$) were used as precursors with distilled water as oxidant. ZrO_2 is one of the most frequently studied materials in ALD, and a wide range of precursors including halides,[19−21] alkoxides,[22,23] β-diketonates,[24] organo-metallics,[25] and alkyl amides[26] have been investigated for ALD of ZrO_2. Among those precursor groups, metal amides have attracted attention for their superior thermal stability, due to strong nitrogen−methyl bonds, and good reactivity to hydroxylated surfaces such as native oxides on silicon wafers due to weak nitrogen−metal bonds.[26] In contrast, there are fewer volatile and thermally stable precursors for ALD of Y_2O_3. A few studies have reported successful ALD of Y_2O_3 using $Y(thd)_3$ (thd = 2,2,6,6-tetramethyl-3,5-hemptadionate),[27] $Y(^iPr_2amd)_3$ ($^iPr_2$-amd = diisopropyl-acetamidinate),[28] $Y(C_5H_5)_3$, and $Y(CH_3C_5H_5)_3$.[29]

A Cambridge NanoTech Savannah 200 reactor customized for 4 in. standard wafers was used in this work. Precursors and oxidants were stored in stainless steel cylinders and heated for source evaporation. There was no transport gas for delivery of evaporated gas into the reaction chamber; rather, precursor vapor was driven by the pressure difference between the source cylinders and the low-pressure chamber. A manual bellows valve throttled the gas outlet of each cylinder. Water vapor and zirconium precursor gas were pulsed into the chamber using solenoid valves. A customized Swagelok ALD diaphragm valve, specially designed for high-temperature operation, was used for the yttrium precursor. All chamber walls were heated to reduce precursor condensation.

The zirconium and yttrium precursors were heated at 100 °C and 190 °C respectively for source evaporation while water was kept at room temperature. We observed $Zr(NMe_2)_4$ precursor decomposition above 250 °C. Therefore, substrate heating with the $Zr(NMe_2)_4$ precursor was limited to a maximum temperature of 250 °C. Deposition was carried out at a pressure of 0.2−0.3 Torr. We used Si_3N_4-buffered Si(100) wafers as substrates. One ALD cycle was executed with the following four steps: (1) pulsing an evaporated precursor into the reaction chamber and chemisorption of the precursor on the substrate, (2) purging reacted ligands and excess unreacted precursor, (3) pulsing the second precursor

followed by surface reaction to form the desired film layer, and (4) purging of byproducts. All depositions were performed in "exposure mode", with all inlets and outlets of the reacting chamber closed for some time to allow sufficient surface reaction. We varied the ratio of zirconium cycles to yttrium cycles to control the composition of YSZ.

For fuel cell fabrication, ALD YSZ films were grown on a Si_3N_4 buffer layer on Si(100) substrates. Prior to depositing YSZ ALD films on silicon substrates, a Si_3N_4 buffer layer was patterned to fabricate open window structures. After YSZ deposition, each patterned window was etched in KOH solution through the entire thickness of the wafer leaving freestanding ALD YSZ and silicon nitride squares with dimensions of tens of micrometers. The thickness of the freestanding silicon nitride layers ranges from 200 nm to 400 nm. After ALD deposition, the supporting silicon nitride layer was removed by plasma assisted chemical etching using SF_6 gas, leaving freestanding YSZ layers. For catalysis and current collection, porous Pt layers were deposited using direct current sputtering on both cathode and anode. For a more detailed description of the fuel cell fabrication process we refer to a recent publication of our group.[7]

Deposited ALD films were characterized either as grown or after annealing at 500−800 °C. Film composition was analyzed by X-ray photoelectron spectroscopy (XPS) in a SSI S-probe monochroma-tized XPS spectrometer with Al Kα radiation (1486 eV). Crystal-linity and phase of the deposited films was analyzed by an X-ray diffraction (XRD) technique using a PANalytical X'Pert PRO XRD system (Cu Kα X-ray with $\lambda = 1.54$ Å), and the symmetrical $\theta/2\theta$ scan method was applied for phase analysis. Film grains were characterized by transmission electron microscopy (TEM). Atomic force microscopy (AFM) images were obtained using a Philips CM20 FEG-TEM system and a JEOL JSPM-5200 system, respec-tively. X-ray reflection (XRR) analysis was performed to determine film density and roughness with the same system used in the XRD analysis. The performance of ALD YSZ membranes as fuel cell electrolytes was measured by obtaining the current−voltage (I−V) relation at temperatures from 265 °C to 350 °C. For the I−V data collection, a Gamry FAS2 Femtostat system was used. To obtain temperature data as accurate as possible, temperature probes were placed in close proximity to the fuel cell. The anode side of the fuel cell sample was sealed on a small chamber where pure dry hydrogen was circulated as fuel. The cathode side was exposed to oxygen in ambient air.

Results and Discussion

Growth rates of zirconia and yttria films deposited at the same temperature (250 °C) were measured individually. Our system delivered a zirconia growth rate of 1.5 Å/cycle, which corresponds well to values reported in literature ($\sim$1−1.7 Å/cycle).[26] The growth rate for yttria was measured to be 3.5 Å/cycle. Although the measured rate for yttria is higher than the published data of 1.2 Å/cycle,[29] film thickness is proportional to number of cycles without precursor decom-position. From the XPS compositional analysis, the yttria content was measured to increase proportionally to the pulse ratio of Y/Zr. From this result, YSZ films with a target stoichiometry (($ZrO_2)_{0.92}(Y_2O_3)_{0.08}$:8% YSZ) were grown by employing a mix of pulse numbers, Zr/Y = 7:1. The XPS system enables us to characterize film composition versus depth with the help of Ar ion surface etching. The resulting depth profile showed the composition of the films as $\sim$7−8% yttria. The composition remains similar through entire

(19) Copel, M.; Gribelyuk, M.; Gusev, E. *Appl. Phys. Lett.* **2000**, *76*, 436−8.
(20) Perkins, C. M.; Triplett, B. B.; McIntyre, P. C.; Saraswat, K. C.; Haukka, S.; Tuominen, M. *Appl. Phys. Lett.* **2001**, *78*, 2357−9.
(21) Kukli, K.; Forsgren, K.; Ritala, M.; Leskela, M.; Aarik, J.; Harsta, A. *J. Electrochem. Soc.* **2001**, *148*, F227−32.
(22) Nakajima, A.; Kidera, T.; Ishii, H.; Yokoyama, S. *Appl. Phys. Lett.* **2002**, *81*, 2824−6.
(23) Chang, J. P.; Lin, Y. S. *J. Appl. Phys.* **2001**, *90*, 2964−9.
(24) Putkonen, M.; Niinisto, J. *J. Mater. Chem.* **2001**, *11*, 3141−7.
(25) Putkonen, M.; Niinisto, J.; Kukli, K.; Sajavaara, T.; Karppinen, M.; Yamauchi, H.; Niinisto, L. *Chem. Vap. Deposition* **2003**, *9*, 207−12.
(26) Hausmann, D. M.; Kim, E.; Becker, J.; Gordon, R. G. *Chem. Mater.* **2002**, *14*, 4350−8.
(27) Putkonen, M.; Sajavaara, T.; Johansson, L. S.; Niinisto, L. *Chem. Vap. Deposition* **2001**, *7*, 44−50.
(28) de Rouffignac, P.; Park, J. S.; Gordon, R. G. *Chem. Mater.* **2005**, *17*, 4808−14.
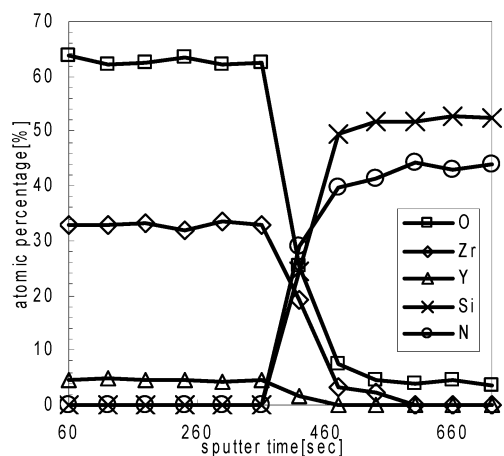(29) Niinisto, J.; Putkonen, M.; Niinisto, L. *Chem. Mater.* **2004**, *16*, 2953−8.

Figure 1. XPS depth profile of ALD YSZ films grown on Si_3N_4 substrates with pulse number ratio Zr/Y = 7:1.
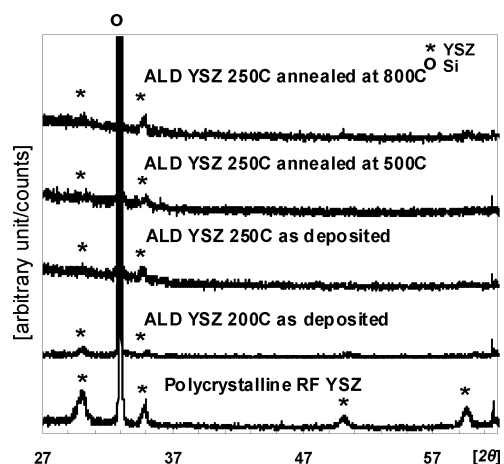

Figure 2. XRD patterns as a function of deposition temperature (200−250 °C), annealing conditions (as-deposited, 500 °C, 800 °C) compared to reference polycrystalline YSZ film prepared by the RF sputtering technique.

Figure 3. Diffraction pattern and TEM image at the film−substrate interface.
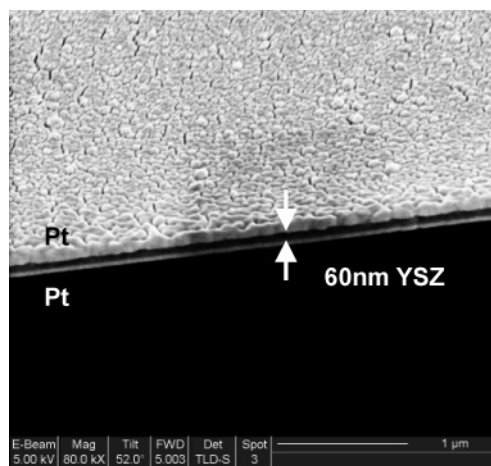
Figure 4. SEM image of freestanding ALD YSZ films with porous Pt cathode−anode layers.

film thickness, as shown in Figure 1. We measured the deposition rate of YSZ to be 2.0 Å/cycle, which was higher than the expected value calculated from the measured rates for ALD of zirconia and yttria. This indicates that oxidation cycles during YSZ growth interact. This phenomenon agrees with previous studies that revealed different growth rates in ALD of ternary oxides from ones in binary oxides with organometallic precursors.[13,17]

In the XRD analysis, the ALD films showed polycrystalline microstructure in agreement with expected diffraction patterns for YSZ (Figure 2). This analysis was performed as a function of deposition temperatures from 200 °C to 250 °C and annealing temperatures from 500 °C to 800 °C. The samples showed a dominant (100) peak. The peaks were broader in films deposited at lower temperature (200 °C). We observed no significant change in crystallinity of films on Si_3N_4, even after high temperature annealing. TEM images confirmed that ALD YSZ films were polycrystalline in an amorphous matrix with grain size of tens of nanometers in the cubic phase (Figure 3). In the AFM analysis, the films were analyzed as deposited or after annealing at 800 °C. The sample as deposited consisted of nanometer sized grains with well-defined grain boundaries. However, the size and shape of the grains hardly changed even after high temperature annealing.
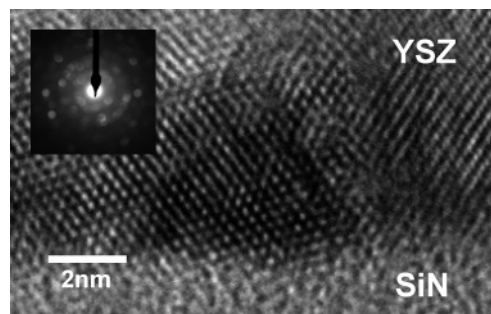
In the XRR analysis, the ALD YSZ film deposited grown on Si_3N_4 surface showed density of 4.8 g/cm³ compared to density of powder processed YSZ known as 5.8−6.1 g/cm³ or the density of ALD films grown directly on Si(100) or quartz substrates which our group found to range from 5.4 g/cm³ to 5.7 g/cm.[30] This volume expansion may be related to the high deposition rate employed for membrane growth as described earlier. Roughness of the films was measured as 2.4 nm for a 140-nm-thick film. Compared to XRR roughness data, the one measured by AFM showed a smaller value (1.5 nm).

We measured the performance of ALD YSZ membranes as fuel cell electrolyte at temperatures from 265 °C to 350 °C. The thickness of the freestanding YSZ layer was 60 nm, while both porous platinum electrodes were 80 nm thick (Figure 4). Scanning electron microscopy (SEM) images were used to measure the active membrane−electrode assembly (MEA) area that ranged from 20 × 20 μm^2 to 100 × 100 μm^2. The best performing cells exhibited a maximum power densities of 270 mW/cm² at 350 °C, 66 mW/cm² at 300 °C, and 28 mW/cm² at 265 °C. A number of cells did not perform at all because of electric shorts between electrodes through the nanoscale electrolyte. The performance of ALD YSZ fuel cells was compared to earlier data published by our group with 50 nm RF-sputtered YSZ films.[7] Open-circuit voltages (OCVs) of the ALD YSZ fuel cells were measured in the range from 1.02 to 1.10 V, close to the ones measured with RF-sputtered films (1.05−1.10 V).

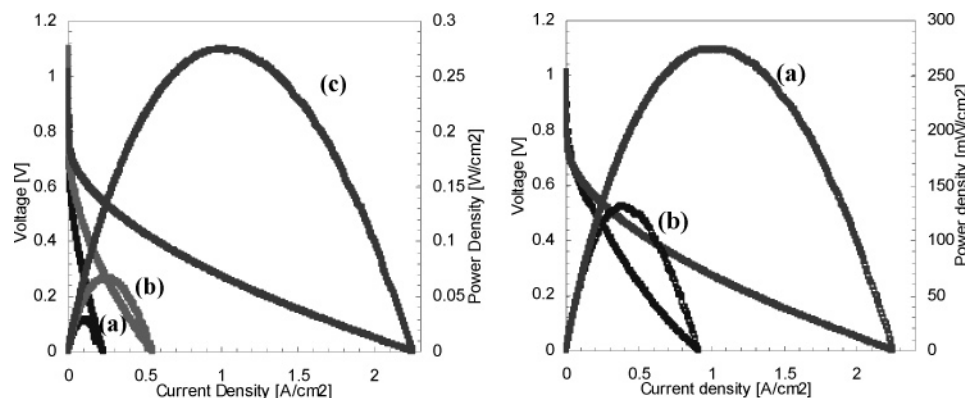(30) Chao, C.; Shim, J. H.; Prinz, F. B. Internal report (not published).

Figure 5. Polarization curves and power density of YSZ fuel cells. (Left) Performance of ALD YSZ fuel cells at (a) 265 °C, (b) 300 °C, and (c) 350 °C. (Right) Performance comparison of (a) ALD YSZ fuel cells to (b) reference fuel cells with 50 nm RF-sputtered YSZ at 350 °C.[7]

We observed a significant increase of maximum power density in fuel cells with ALD electrolytes relative to the ones with RF sputtered electrolyte membranes (Figure 5).

The $I-V$ curves were evaluated through numerical approximation to a standard polarization model including activation and ohmic losses.[31] Excluding losses due to mass transport, the resulting fuel cell output voltage associated with drawing current can be described as

$$V_{cell} = V_{ocv} - \eta_{electrodes} - j\text{ASR} \tag{1}$$

where V_{ocv} is the Nernstian OCV, $\eta_{electrodes}$ is the overpotential at the electrodes, j is the current density, and ASR is the electrolyte area specific resistance. At currents higher than the exchange current density (j_0), dependency of the electrode overpotential on current can be represented by the following Tafel equation, which describes the activation losses:

$$\eta_{electrodes} = \frac{RT}{\alpha n F} \ln \frac{j}{j_0} \tag{2}$$

where α is the charge-transfer coefficient, j is the generated current density, and R, T, and F have their usual meanings. Performing a best fit of the $I-V$ data to the Tafel equation yielded values for α of 0.53. The ASR values were determined as 2.3, 0.99, and 0.24 Ω cm^2 at 265, 300, and 350 °C, respectively, and the activation energy yield of 0.86 eV is similar to earlier measurements of 0.88 eV.[32] The ASR can be scaled down by thinning the membrane, while the exchange current density and the transfer coefficient are not expected to depend on film thickness. Thus, the performance enhancement is expected to primarily originate from reduced ohmic loss in ultrathin electrolytes. However, estimation of j_0 by the Tafel equation in the present experiments showed a significant increase in exchange current density by about 4 orders of magnitude compared to the reference plots extrapolated from published Pt-YSZ values[32] (Figure 6).

In our previous experiments with 50 nm RF sputtered YSZ, we also observed enhanced charge-transfer kinetics on the nanocrystalline YSZ compared to bulk YSZ.[7] This phenomenon could be caused by enhanced oxygen exchange
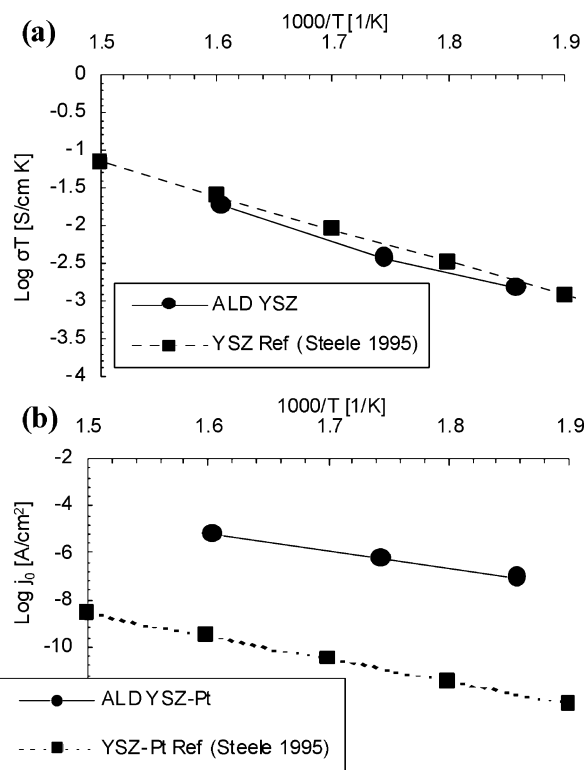

Figure 6. Measured (a) ionic conductivity [σ] and (b) exchange current density [j_0] of ALD YSZ with porous Pt in comparison with plots extrapolated from reference data.[32]

rates on the surface of nanocrystalline YSZ that were 2 orders of magnitude higher than that on the bulk YSZ suggesting better catalytic properties of oxygen dissociation on nanocrystalline YSZ surfaces.[33] We also observed that the overall performance of the ALD fuel cell was even higher than one containing the RF sputtered nanocrystalline membrane.[7] This additional enhancement could be related to the nanograin morphology of ALD YSZ films, which is currently under investigation.

Conclusion

Successful synthesis of nanoscale oxide ion-conducting YSZ with optimal Y/Zr composition by the ALD technique was demonstrated for the first time. Structural characteristics

(31) O'Hayre, R.; Cha, S.; Colella, W.; Prinz, F. B. *Fuel Cell Fundamentals*; John Wiley and Sons: New York, 2006.
(32) Steele, B. C. H. *Solid State Ionics* **1995**, *75*, 157−65.

(33) Knoner, G.; Reimann, K.; Rower, R.; Sodervall, U.; Schaefer, H. E. *Proc. Natl. Acad. Sci. U.S.A.* **2003**, *100*, 3870−3.

of ALD YSZ films grown on amorphous Si_3N_4 showed that they were polycrystalline with volume expansion confirmed by XRD, XRR, and TEM techniques and fine spherical grains by AFM images. Fuel cell performance data between 265 and 350 °C showed maximum power densities of 28−270 mW/cm², respectively. Performance enhancement origi-

nated from an increase in exchange current density at the electrode−electrolyte interface.